

Nanoscale

Accepted Manuscript



This is an *Accepted Manuscript*, which has been through the Royal Society of Chemistry peer review process and has been accepted for publication.

Accepted Manuscripts are published online shortly after acceptance, before technical editing, formatting and proof reading. Using this free service, authors can make their results available to the community, in citable form, before we publish the edited article. We will replace this *Accepted Manuscript* with the edited and formatted *Advance Article* as soon as it is available.

You can find more information about *Accepted Manuscripts* in the [Information for Authors](#).

Please note that technical editing may introduce minor changes to the text and/or graphics, which may alter content. The journal's standard [Terms & Conditions](#) and the [Ethical guidelines](#) still apply. In no event shall the Royal Society of Chemistry be held responsible for any errors or omissions in this *Accepted Manuscript* or any consequences arising from the use of any information it contains.

COMMUNICATION

Nanoscale Mapping of Catalytic Activity Using Tip-enhanced Raman Spectroscopy

Cite this: DOI: 10.1039/x0xx00000x

N. Kumar^a, B. Stephanidis^b, R. Zenobi^b, A. J. Wain^{*c} and D. Roy^{*a}Received 00th January 2012,
Accepted 00th January 2012

DOI: 10.1039/x0xx00000x

www.rsc.org/nanoscale

Chemical mapping of a photocatalytic reaction with nanoscale spatial resolution is demonstrated for the first time using tip-enhanced Raman spectroscopy (TERS). An ultrathin alumina film applied to the Ag-coated TERS tip blocks catalytic interference whilst maintaining near-field electromagnetic enhancement, thus enabling spectroscopic imaging of catalytic activity on nanostructured Ag surfaces.

The development of new catalyst materials with improved efficiency and selectivity is underpinned by a molecular understanding of reactive surface phenomena. Traditionally, catalyst development has been based largely on macroscopic studies; however a paradigm shift towards rational design of nanostructured catalysts with tailored properties demands nanoscale techniques to deepen our grasp of the associated interfacial processes. The properties of catalytic interfaces are known to be spatially heterogeneous¹, and hence measuring the distribution of activity across a surface and establishing its relationship with bulk performance is essential to optimising new materials for this and a wide range of other applications. Conventional analytical techniques such as molecular vibrational spectroscopy offer critical insights into catalytic processes via identification of adsorbates and reaction intermediates, but they often lack sensitivity and in many cases fail to reveal useful information about the spatial distribution of active sites at the necessary length scale. A prime example is Raman spectroscopy, which is a widely-used technique for *in situ* characterisation of heterogeneous catalysts and monitoring of chemical reactions^{2,3}, but suffers from the above limitations. Whilst the problem of low sensitivity can be resolved using resonance Raman or surface-enhanced Raman spectroscopy (SERS), the spatial resolution is diffraction-limited and therefore cannot be overcome using conventional far-field techniques⁴. Hence, nanoscale monitoring of reactions at a single catalytically-active particle remains a significant challenge.

Tip-enhanced Raman spectroscopy (TERS) has emerged as a powerful and reliable technique for chemical characterisation of surfaces at the nanoscale, which combines the high chemical sensitivity of SERS and high spatial resolution of scanning probe microscopy (SPM)⁵⁻⁷. When a metal or metal-coated SPM tip is placed at the centre of a focused laser spot, the localised surface

plasmon (LSP) resonance at the tip-apex enhances the electromagnetic (EM) field within a distance of a few nanometres⁸. This EM enhancement causes an increase in Raman signal intensity obtained from the analyte molecules in the immediate vicinity of the tip-apex, enabling a spatial resolution far beyond the diffraction limit. TERS has been successfully used to gain novel insights in a wide variety of research areas such as photovoltaics⁹, single-wall carbon nanotubes¹⁰, semiconductors¹¹, biology¹², graphene¹³ and single molecule detection¹⁴. Despite the recognised advantages^{4, 15} only a handful of TERS studies of catalytic reactions have been reported to date^{16, 17}. Most notably, nanoscale monitoring of a photocatalytic reduction reaction using TERS was reported by Lantman *et al.*¹⁷ on an ultraflat Au nanoplate substrate. The authors observed the change in Raman spectrum from reactants to products in the near-field from *in situ* time-series spectra. However, high-resolution chemical mapping was not carried out in this study and further technique development is clearly required.

Plasmon-assisted heterogenous catalysis¹⁸⁻²⁰ has attracted significant attention recently, in which LSP resonance in metal nanostructures facilitates charge-transfer photochemistry^{21, 22} via enhancement in the local EM field intensity^{23, 24}. This LSP resonance, which occurs only when the frequency of the excitation laser matches the characteristic plasmon frequency of the metal nanostructures, generates hot electrons and hot holes at the metal surface and has been reported to activate the adsorbed molecules and catalyse chemical reactions²⁵. Raman spectroscopy is a powerful technique to investigate such photocatalytic reactions. For example, *in situ* monitoring of the plasmon-assisted reduction of 4-nitrothiophenol (4-NTP) to *p, p'*-dimercaptoazobenzene (DMAB) on single Ag microflower particles was demonstrated by Tang *et al.* using time-dependent SERS²⁶. The same reaction was also the focus of the aforementioned TERS study.¹⁷ Another prevalent, and closely related, example is the plasmon-enhanced photocatalytic oxidation of *p*-mercaptoaniline (pMA) to DMAB (Fig. 1a)²⁵, which can be monitored by Raman spectroscopy due to distinct azo bands in the region 1140 to 1500 cm⁻¹^{27, 28}. Given the recent attention received by such reactions in the context of understanding plasmon-enhanced coupling, the oxidative dimerisation of pMA to DMAB on nanostructured silver was selected as a model reaction for the demonstration of high-resolution spectroscopic imaging.

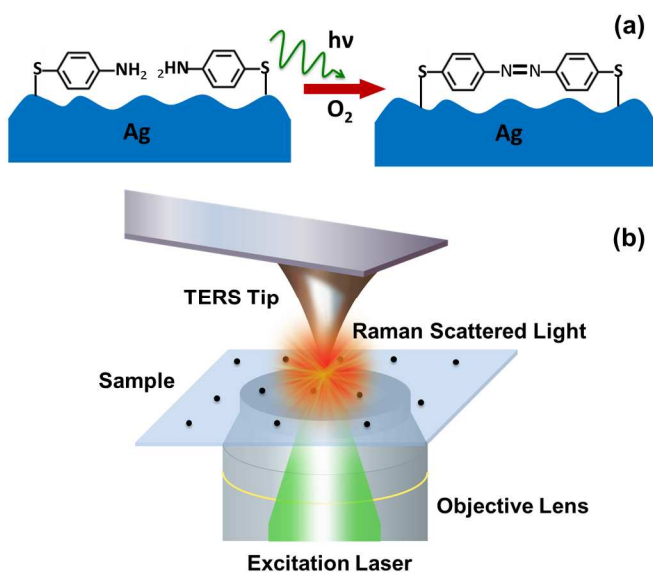


Fig. 1 (a) Schematic diagram of the photocatalytic oxidation of pMA to DMAB in which pMA molecules, chemically bound to an Ag substrate *via* their thiol group, undergo coupling upon photoexcitation. Under ambient conditions, the reaction occurs via plasmon-assisted surface catalysis in which O_2 adsorbed on Ag surface first gets activated by hot electrons created by LSP resonance and subsequently reacts with adsorbed pMA molecules to form DMAB²⁵. (b) Schematic depiction of the transmission-mode atomic force microscopy (AFM)-TERS apparatus used in this work.

Herein, for the first time we present nanoscale Raman mapping of this photocatalytic reaction occurring at an isolated catalytic point using an Ag-coated TERS tip in an AFM-TERS configuration. Since, in this case, the plasmonic properties of Ag have the dual effect of spectroscopic enhancement and photocatalytic activity, the use of Ag-coated TERS tips for mapping catalytic surfaces is problematic. Therefore, in this work we show that, by protecting the TERS tip with an ultrathin alumina film, the interaction of Ag with the analyte molecules can be blocked while maintaining its plasmonic enhancement. Finally, we demonstrate that the alumina-protected TERS tips enable nanoscale mapping of the photocatalytic activity of nanostructured Ag substrates.

The TERS system used in this work is shown schematically in Fig. 1b. Measurements were conducted in contact-mode AFM on a home-built transmission mode TERS system consisting of an AFM (AIST-NT, The Netherlands) placed on top of an inverted confocal microscope (Nikon, Japan). All near-field and far-field spectra were recorded using a spectrometer (iHR 320, HORIBA Scientific, U.K.) fitted with an EMCCD camera (Newton, Andor, Belfast). A radially polarised excitation laser of 532 nm was focused on to the sample using a 100 \times , 1.49 NA oil immersion objective lens (Nikon, Japan). A low laser power of 10 μ W at the objective was used for all measurements. TERS tips were prepared by thermally evaporating 40 nm Ag onto contact mode Si AFM tips (Mikromasch, Estonia) in a vacuum chamber at 10⁻⁶ mbar pressure at a slow deposition rate of 0.05 nm/s.

We begin with the spectroscopic mapping of the photocatalytic reaction at an Ag-coated TERS tip-apex. This was achieved by contacting the tip to a glass coverslip (thickness \approx 0.17 mm) coated with a thin film of pMA embedded in poly(methyl methacrylate) (PMMA). The thin film was prepared by spin-coating a solution of 3 mg/mL of pMA and 10 mg/mL of PMMA dissolved in chloroform at 2000 revolutions per minute for one minute. The

thickness of the film was measured to be 50 nm by imaging a scratch on the film using a calibrated AFM. An objective lens mounted on an XYZ scanner was used to collect Raman spectra from a raster map of 20 \times 20 pixels from an area of 1 μ m \times 1 μ m around the stationary TERS tip. The Raman intensity at 1142 cm^{-1} , which is attributed to the C-N stretching vibration of DMAB^{27,28}, was used to generate the map shown in Fig. 2a, in which the highest intensity of the DMAB band is located at position A, which marks the single point at which the Ag-coated tip contacts the film. Fig. 2b shows the near-field spectrum recorded at position A (Spectrum 1), which contains all of the characteristic Raman peaks of DMAB²⁷. Spectrum 2 in Fig. 2b is the far-field spectrum recorded at location B in the Raman map and shows the characteristic bands of pMA alone, indicating that the reaction pMA \rightarrow DMAB occurs only at the tip-apex. It should be noted that the integration time for spectra 1 and 2 are 0.5 s \times 1 accumulation (acc.) and 10 s \times 18 acc., respectively. The much higher signal to noise ratio in spectrum 1, acquired over a much shorter integration time, indicates that the TERS tip not only acts as a catalyst for the reaction but is also responsible for a significant near-field Raman signal enhancement. Fig. 2b also shows the far-field spectrum (Spectrum 3) collected from position A with the TERS tip retracted away from the sample. Spectrum 3 matches exactly with Spectrum 2, confirming the necessity for contact between the Ag-coated TERS tip and the surface for the occurrence of photocatalytic reaction and for the near-field Raman signal enhancement.

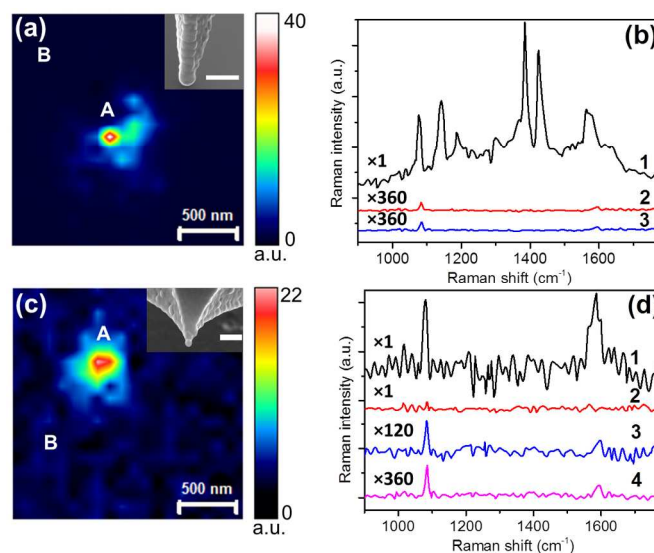


Fig. 2. (a) Mapping of photocatalytic reaction occurring at the Ag-coated TERS tip-apex using the 1142 cm^{-1} peak intensity of DMAB. SEM image of the tip is shown in the inset. Scale bar: 100 nm. (b) 1) Near-field spectrum from position A in Fig. 2a with the tip in contact with the pMA/PMMA surface. Integration time: 0.5 s \times 1 accumulation. 2) Far-field spectrum from position B in Fig. 2a with the tip in contact with the surface. Integration time: 10 s \times 18 acc. 3) Far-field spectrum from position A in Fig. 2a with tip retracted away from the surface. Integration time: 10 s \times 18 acc. (c) Raman mapping of the alumina-protected Ag-coated TERS tip-apex using the 1086 cm^{-1} peak intensity of pMA²⁸. SEM image of the tip is shown in the inset. Scale bar: 100 nm. (d) 1) Near-field spectrum from position A in Fig. 2c with tip in contact with the surface. Integration time: 0.5 s \times 1 acc. 2) Far-field spectrum from position B in Fig. 2c with tip in contact with the surface. Integration time: 0.5 s \times 1 acc. 3) Far-field spectrum from position B in Fig. 2c with tip in contact with the surface. Integration time: 10 s \times 6 acc. 4) Far-field spectrum from position A in Fig. 2c with tip retracted away from the surface. Integration time: 10 s \times 18 acc.

The fact that the Ag-coated TERS tips are themselves catalytically active creates an inherent problem in using them to map the activity of a catalytic surface. For TERS mapping, it was therefore necessary to protect the Ag from physical exposure to the pMA molecules without sacrificing the plasmonic signal enhancement. This was achieved by adding a chemically blocking layer of alumina to the outside of the Ag-coated TERS tips. In this case 50 nm of Ag was first thermally evaporated onto silicon nitride AFM tips (Olympus, Japan), and the resulting probes were subsequently protected with a 3-5 nm thick layer of alumina deposited by 25 cycles of atomic layer deposition (ALD) at 120 °C. Fig. 2c shows the Raman map acquired around the alumina-protected tip contacting the same sample as for Fig. 2a, but using the 1086 cm⁻¹ Raman peak, which is attributed to the ν_{CC} vibrational mode of pMA²⁸ to construct the map. Raman spectra recorded at positions A and B in Fig. 2c, with the tip in contact with the surface, are shown in Fig. 2d (spectra 1 and 2 respectively). Importantly, none of the peaks associated with DMAB were observed, indicating that the photocatalytic reaction pMA → DMAB was successfully blocked. Comparing the spectra from position A and B, both of which were collected for 0.5 s, a significant enhancement of the pMA Raman signal can be observed at the apex of the alumina-protected tip. Only after increasing the integration time to 10 s × 6 acc., are we able to observe the pMA peaks at position B (Spectrum 3). Moreover, the far-field spectrum from position A (Spectrum 4) also shows the characteristic peaks of the

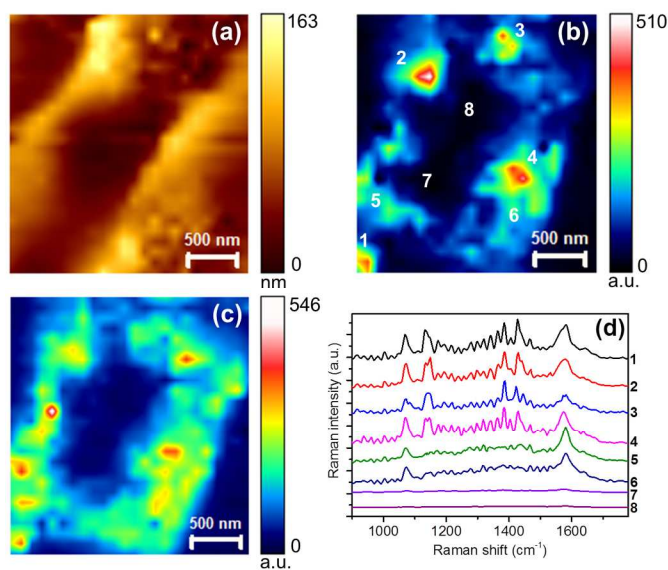


Fig. 3 (a) Topography image of the patterned Ag substrate. (b) TERS map showing the variation of 1142 cm⁻¹ Raman peak intensity of DMAB. (c) TERS map showing the variation of 1595 cm⁻¹ Raman peak²⁸ intensity of pMA. (d) Near-field spectra from the positions marked in (b). Integration time: 0.5 s.

pMA with an integration time of 10 s × 18 acc. Hence, the alumina protection of the Ag-coated TERS tip prevents the photocatalytic reaction at the tip-apex, further confirming the catalytic role of Ag in the pMA → DMAB reaction. Furthermore, comparison of the signal to noise ratio of near-field spectra in Fig. 2b and 2d shows that, although EM enhancement at the Ag tip-apex is diminished by the alumina coating, it is still significant compared to the far-field Raman signal. The enhancement factor (EF) is usually calculated using the following relation²⁹

$$EF = \left(\frac{I_{NF}}{I_{FF}} - 1 \right) \frac{A_{FF}}{A_{NF}}, \quad (1)$$

where I_{NF} and I_{FF} are Raman peak intensities in the near-field and far-field, respectively; A_{FF} and A_{NF} are the areas of far-field and near-field, which are estimated from the size of the laser spot and TERS tip-apex, respectively. In our TERS system the diameter of laser-spot was measured to be ~450 nm and size of the tip-apex was measured from the SEM image to be ~50 nm (Fig. 2c). Using these values the EF of the alumina-protected TERS tip for the 1086 cm⁻¹ Raman peak of pMA is calculated to be ~10⁵.

The EM enhancement and lack of catalytic activity offered by the alumina-protected Ag-coated TERS tips were utilised to map the distribution of catalytic activity of a patterned Ag substrate prepared by thermal evaporation onto a glass coverslip using 3 μm silica beads as sacrificial shadow masks (Fig. 3). pMA molecules were adsorbed on the Ag substrate by immersing it in a 5 mM solution of pMA in ethanol for 2 hours, immediately after removal from the evaporation chamber. Fig. 3a shows the topography image (26×24 pixels) acquired during TERS mapping of the sample which, in addition to various surface features, exhibits a dark (Ag-free) region at the centre, as well as in the top-left and bottom-right corners. TERS maps generated using the 1142 cm⁻¹ DMAB Raman peak intensity and 1595 cm⁻¹ pMA peak²⁸ (attributed to the $\nu_{CC} + \nu_{CS}$ vibrational modes of pMA and which overlaps with the 1578 cm⁻¹ DMAB peak²⁷) are presented in Figures 3b and 3c respectively and indicate no detectable adsorbates in the Ag-free regions of the sample. Furthermore, a comparison of these TERS maps indicates that, although the Ag surface is covered with the pMA molecules (Figure 3c), the reaction pMA → DMAB occurs only at certain locations on the sample (Figure 3b), presumably where the LSP resonance with the excitation laser takes place leading to the creation of hot electrons. This is shown in the near-field Raman spectra (Fig. 3d) measured from the positions marked in Fig. 3b. The Raman peaks from the product DMAB are present only in the spectra from positions 1-4 indicating the occurrence of photocatalytic reaction only at these places. Conversely, the DMAB Raman peaks are absent from the near-field spectra at positions 5 and 6, which only show the Raman peaks of unreacted pMA adsorbed on the Ag substrate. Furthermore, all Raman bands are absent in the spectra from positions 7 and 8, which represent the regions where no silver was present on the substrate, indicating that the pMA molecules adsorb only at the silver surface.

Finally, we carried out high resolution TERS mapping of the pMA → DMAB reaction on a substrate coated with Ag nanoparticles. This sample was prepared by depositing a thin-film (≈10 nm) of Ag onto a glass coverslip by thermal evaporation inside a vacuum chamber at 10⁻⁶ mbar pressure and produced a uniform film of Ag nanoparticles with sizes ranging from 5 – 40 nm (Fig 4a). Immediately after removal from the evaporation chamber, pMA molecules were adsorbed on the Ag substrate by immersing it in a 5 mM solution of pMA in ethanol for 2 hours. Since the Ag substrate contains a range of Ag nanoparticle sizes, only a fraction of them are expected to have LSP in resonance with the 532 nm laser and hence show catalytic activity towards the plasmon-assisted pMA oxidation reaction²⁵. Fig. 4b shows the TERS map from the area marked with dotted rectangle in Fig. 4(a), generated using the 1142 cm⁻¹ peak of DMAB.

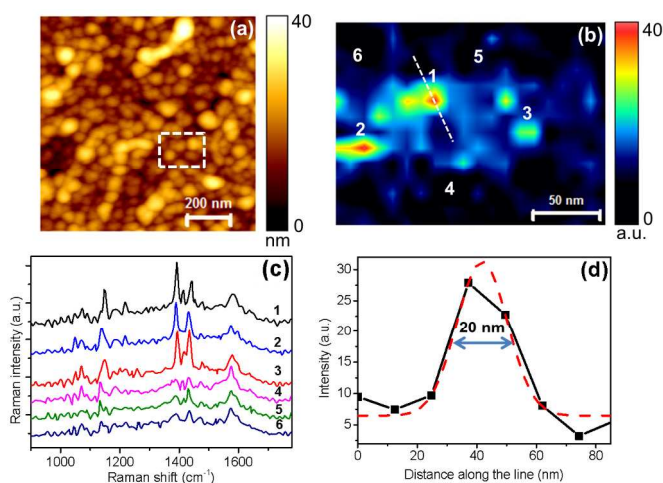


Fig. 4 (a) AFM topography image of an Ag substrate with Ag nanoparticles on a glass substrate. (b) TERS map from the dashed rectangle marked in (a), showing the variation of the 1142 cm^{-1} Raman peak intensity of DMAB. (c) Near-field spectra from the positions marked in (b). Integration time: 0.5 s. (d) Intensity profile along the dotted line marked in (b) showing the spatial resolution of the TERS map. Gaussian fit to the intensity profile is shown by the dashed red curve.

It is noted that the photocatalytic reaction $\text{pMA} \rightarrow \text{DMAB}$ takes place only at a few locations on the Ag substrate, which are evident with a high intensity of the 1142 cm^{-1} Raman peak of DMAB. For example, TERS spectra from positions 1, 2 and 3 shown in Fig. 4c exhibit intense DMAB signature peaks, whilst these peaks are almost entirely absent or have much weaker intensity at positions 4, 5 and 6. This highlights the heterogeneous nature of this surface, which exhibits regions of high and low photocatalytic activity towards this model reaction²⁵. These regions of high Raman signals, associated with high density of active sites on the surface, can only be differentiated due to the high spatial resolution and sensitivity of the TERS technique. Fig. 4d shows the intensity profile along the dotted line across one such catalytically-active region and the full width half maximum (FWHM) of a Gaussian curve fitted to this profile indicated that the resolution of the TERS map may be as small as 20 nm.

Conclusions

Despite the potential of TERS to study catalytic reactions with a high resolution^{4,15}, few systems have been investigated so far. The results presented in this work demonstrate that the high chemical sensitivity and nanoscale spatial resolution of TERS makes it ideally suited for the characterisation of heterogeneous catalytic reactions. For the first time, we have mapped a catalytic reaction occurring at a single point of contact between a TERS tip and a reactant substrate. Moreover, the use of an alumina-coated TERS tip to enhance the Raman signal while inhibiting the direct photocatalytic reaction at the tip-apex, has enabled mapping of the distribution of catalytic activity across Ag substrates with submicron and nanoscale structures. In this case, TERS has allowed differentiation between catalytically-active and inactive particles with 20 nm spatial resolution. Such high-resolution chemical mapping of catalytically active surfaces has not been achieved by any other analytical technique. This work is expected to pave the way for the routine use of TERS for studying catalytic reactions with nanoscale spatial resolution, and ultimately spectroscopic mapping of individual catalytic sites.

Acknowledgements

NK, DR and AW acknowledge the EMRP IND15 project ‘SurfChem’, and DR, BS and RZ acknowledge financial support from the EMRP NEW02 project ‘Metrology for Raman spectroscopy’. The EMRP is jointly funded by the participating countries within EURAMET and the European Union.

Notes and references

^a Analytical Science Division, National Physical Laboratory, Hampton Road, Teddington, Middlesex, TW11 0LW, UK. Email: debdul.roy@npl.co.uk

^b Department of Chemistry and Applied Biosciences, Laboratory of Organic Chemistry, ETH Zurich, 8093 Zurich, Switzerland

^c Materials Division, National Physical Laboratory, Hampton Road, Teddington, Middlesex, TW11 0LW, UK. Email: andy.wain@npl.co.uk

†Electronic Supplementary Information (ESI) available: See DOI: 10.1039/c000000x/

- I. L. C. Buurmans and B. M. Weckhuysen, *Nat. Chem.*, 2012, **4**, 873-886.
- B. M. Weckhuysen, *In-situ spectroscopy of catalysts*, American Scientific Publishers Stevenson Ranch, CA, 2004.
- G. Mestl, *J. Mol. Catal. A-Chem.*, 2000, **158**, 45-65.
- H. Kim, K. M. Kosuda, R. P. Van Duyne and P. C. Stair, *Chemical Society Reviews*, 2010, **39**, 4820-4844.
- T. Schmid, L. Opilik, C. Blum and R. Zenobi, *Angew. Chem. Int. Ed.*, 2013, **52**, 5940-5954.
- C. Blum, L. Opilik, J. M. Atkin, K. Braun, S. B. Kammer, V. Kravtsov, N. Kumar, S. Lemeshko, J. F. Li, K. Luszcz, T. Maleki, A. J. Meixner, S. Minne, M. B. Raschke, B. Ren, J. Rogalski, D. Roy, B. Stephanidis, X. Wang, D. Zhang, J. H. Zhong and R. Zenobi, *J. Raman Spectrosc.*, 2014, **45**, 22-31.
- A. J. Pollard, N. Kumar, A. Rae, S. Mignuzzi, W. Su and D. Roy, *Journal of Materials NanoScience*, 2014, **1**, 39-49.
- F. Festy, A. Demming and D. Richards, *Ultramicroscopy*, 2004, **100**, 437-441.
- X. Wang, D. Zhang, K. Braun, H. J. Egelhaaf, C. J. Brabec and A. J. Meixner, *Adv. Funct. Mater.*, 2010, **20**, 492-499.
- Y. Okuno, Y. Saito, S. Kawata and P. Verma, *Phys. Rev. Lett.*, 2013, **111**, 216101.
- N. Lee, R. D. Hartschuh, D. Mehtani, A. Kisliuk, J. F. Maguire, M. Green, M. D. Foster and A. P. Sokolov, *J. Raman Spectrosc.*, 2007, **38**, 789-796.
- S. Najjar, D. Talaga, L. Schue, Y. Coffinier, S. Szunerits, R. Boukherroub, L. Servant, V. Rodriguez and S. Bonhommeau, *J. Phys. Chem. C*, 2014, **118**, 1174-1181.
- W. Su and D. Roy, *J. Vac. Sci. Technol., B*, 2013, **31**, 041808.
- R. Zhang, Y. Zhang, Z. C. Dong, S. Jiang, C. Zhang, L. G. Chen, L. Zhang, Y. Liao, J. Aizpurua, Y. Luo, J. L. Yang and J. G. Hou, *Nature*, 2013, **498**, 82-86.
- C. E. Harvey and B. M. Weckhuysen, *Catalysis Letters*, 1-18.
- K. F. Domke and B. Pettinger, *Chemphyschem*, 2009, **10**, 1794-1798.
- E. M. van Schroyenstien Lantman, T. Deckert-Gaudig, A. J. G. Mank, V. Deckert and B. M. Weckhuysen, *Nature Nanotechnology*, 2012, **7**, 583-586.
- X. M. Zhang, Y. L. Chen, R. S. Liu and D. P. Tsai, *Reports on Progress in Physics*, 2013, **76**, 41.
- X. Manda, J. Ruibin, W. Feng, F. Caihong, W. Jianfang and J. C. Yu, *J. Mater. Chem. A*, 2013, **1**, 5790-5805.
- S. Linic, P. Christopher and D. B. Ingram, *Nat. Mater.*, 2011, **10**, 911-921.

Journal Name

21. L. Brus, *Accounts of Chemical Research*, 2008, **41**, 1742-1749.
22. C. D. Lindstrom and X. Y. Zhu, *Chem. Rev.*, 2006, **106**, 4281-4300.
23. M. Moskovits, *Reviews of Modern Physics*, 1985, **57**, 783-826.
24. K. Watanabe, D. Menzel, N. Nilius and H. J. Freund, *Chem. Rev.*, 2006, **106**, 4301-4320.
25. L. B. Zhao, M. Zhang, Y. F. Huang, C. T. Williams, D. Y. Wu, B. Ren and Z. Q. Tian, *Journal of Physical Chemistry Letters*, 2014, **5**, 1259-1266.
26. X. H. Tang, W. Y. Cai, L. B. Yang and J. H. Liu, *Nanoscale*, 2014, **6**, 8612-8616.
27. Y.-F. Huang, H.-P. Zhu, G.-K. Liu, D.-Y. Wu, B. Ren and Z.-Q. Tian, *J. Am. Chem. Soc.*, 2010, **132**, 9244-9246.
28. D. Y. Wu, X. M. Liu, Y. F. Huang, B. Ren, X. Xu and Z. Q. Tian, *J. Phys. Chem. C*, 2009, **113**, 18212-18222.
29. N. Kumar, A. Rae and D. Roy, *Appl. Phys. Lett.*, 2014, **104**, 123106.